Isolation and characterization of tumorspheres from a recurrent pineoblastoma patient: Feasibility of a patient-derived xenograft

JIYONG KWAK[1*], JIN-KYOUNG SHIM[2*], DONG SEOK KIM[2*], JI-HYUN LEE[2], JUNJEONG CHOI[3], JUNSEONG PARK[2], KYOUNG-JIN SHIN[4], SE-HOON KIM[5], PILNAM KIM[6], YONG-MIN HUH[7], EUI HYUN KIM[2], JONG HEE CHANG[2], SUN HO KIM[2] and SEOK-GU KANG[2]

Departments of [1]Medical Science, [2]Neurosurgery, Brain Tumor Center, Severance Hospital, Yonsei University College of Medicine, Seoul; [3]Department of Pharmacy, College of Pharmacy, Yonsei Institute of Pharmaceutical Sciences, Yonsei University, Incheon; Departments of [4]Forensic Medicine, [5]Pathology, Severance Hospital, Yonsei University College of Medicine, Seoul; [6]Department of Bio and Brain Engineering, Korea Advanced Institute of Science and Technology, Daejeon; [7]Department of Radiology, Severance Hospital, Yonsei University College of Medicine, Seoul, Republic of Korea

Received March 15, 2016; Accepted April 25, 2016

DOI: 10.3892/ijo.2016.3554

Abstract. The existence of tumorspheres (TSs) might confer treatment resistance to pineoblastoma (PB). The existence of PB TSs with cellular immortalization potential has not yet been reported. We developed a procedure for isolating TSs from recurrent PB (rPB) and tested whether their properties made them suitable for use as a patient-derived xenograft (PDX). Immunocytochemical staining, RT-PCR and quantitative real-time PCR showed that, among stemness proteins, CD133, musashi and podoplanin were expressed at elevated levels in rPB TSs, but nestin was not. rPB TSs cultured under neuro-glial differentiation conditions expressed TUBB3, but not GFAP, MBP or NeuN. Unlike glioblastoma TSs, rPB TSs showed no clear evidence of invasion in 3D invasion assay or increased expression of genes associated with epithelial-mesenchymal transition. An orthotopic xenograft showed that tumor xenografts replicated the histopathological features of the patient tumor and expressed similar genome profiles, as determined by short tandem repeat genotyping. These data demonstrate the isolation and the characterization of rPB TSs for the first time. Using an orthotopic xenograft, we showed that rPB TSs could replicate the patient tumor, demonstrating their potential as a PDX for precision medicine.

Correspondence to: Professor Seok-Gu Kang, Department of Neurosurgery, Severance Hospital, Yonsei University College of Medicine, 50-1 Yonsei-ro, Seodaemun-gu, Seoul 120-752, Republic of Korea
E-mail: seokgu9@gmail.com

*Contributed equally

Abbreviations: CSC, cancer stem cell; PDX, patient-derived xenograft; rPB, recurrent pineoblastoma; TS, tumorsphere

Key words: cellular immortalization, patient-derived xenograft, pineoblastoma, stemness, tumorsphere

Introduction

Pineal parenchymal cells in the brain, which are distinct from neuronal and glial cells, can give rise to tumors such as pineocytomas and malignant pineoblastomas (PBs) (1). PB is a highly malignant, primitive embryonal tumor of the pineal gland with a predilection for children (2). PBs account for only 0.6% of pediatric brain tumors, but they display aggressive behavior that is associated with low survival rates (3). Studies have shown that the 5-year survival rate of PB patients is 58% (4), and the median survival following surgical intervention is 25.7 months (5). We believe that the poor clinical outcome for PB patients might be attributable to the effect of refractory cells that show resistance to the current mode of treatment (6,7).

Previous studies have suggested that a distinct population of tumor-initiating cells known as cancer stem cells (CSCs) exist in cancers such as leukemia (8), solid tumors of epithelial origin (9), glioblastomas (GBMs) (10,11) and medulloblastomas (10-14). These cells are characterized by their ability to self-renew and form secondary tumorspheres (TSs), ability to undergo limited multipotent differentiation, and successful tumorigenesis upon implantation (11,12,15). It has been suggested that the incomplete elimination of these TSs may give rise to cancer recurrence (16-18). To the best of our knowledge, isolation of TSs from recurrent PB (rPB) has not been reported. We confirmed our hypothesis that TSs could be isolated from rPB and assessed their stemness, neuro-glial differentiation and invasion characteristics in comparison with TSs from GBM. A mouse orthotopic xenograft model was established to compare histopathological properties and DNA fingerprint with the original patient tumor. In the present study, we report the isolation and the characterization of rPB TSs for cellular immortalization in an rPB patient.

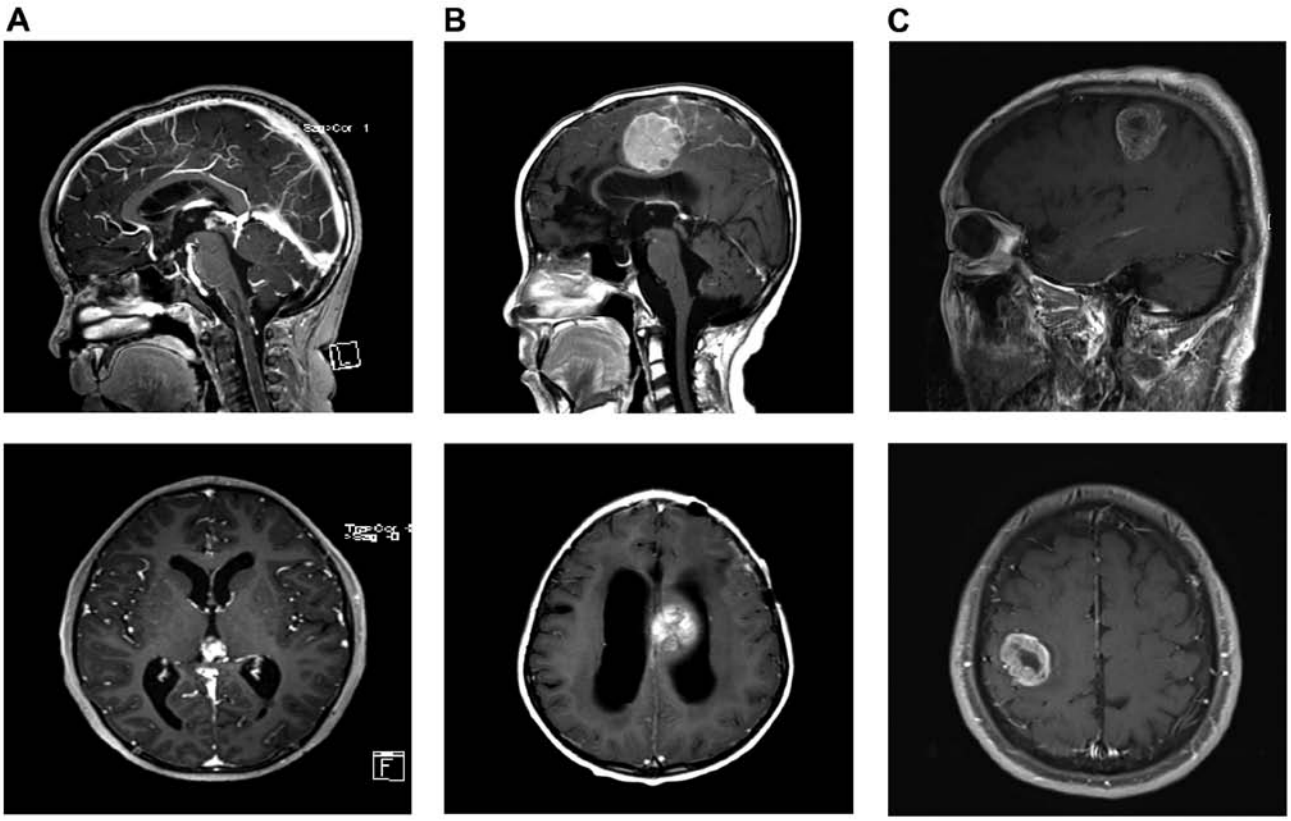

Figure 1. Patient images. (A) Images of the initial PB. MRI showed enhanced pineal mass with hydrocephalus. Top, T1 sagittal, enhanced; bottom, T1 axial, enhanced. (B) Images of rPB. MRI showed enhanced left fronto-parietal mass that was compressing the corpus callosum with hydrocephalus. Top, T1 sagittal, enhanced; bottom, T1 axial, enhanced. (C) Images of GBM. MRI showed enhanced mass with internal necrosis along the right corona radiate in the right perirolandic area. Top, T1 sagittal, enhanced; bottom, T1 axial, enhanced.

Materials and methods

Patient clinical information. A 6-year-old male patient was admitted to the hospital for headache, nausea and vomiting, which had continued for 1 month. Magnetic resonance imaging (MRI) revealed a solid mass in the pineal region with hydrocephalus (Fig. 1A). The patient underwent a series of chemotherapy and radiation therapy following endoscopic third ventriculostomy and biopsy, which were diagnosed as PB. The tumor recurred on the left frontal lobe 10 months after the initial therapy and was removed using an occipital transtentorial approach. The final pathological diagnosis was also consistent with PB. A year later, the tumor recurred in the fronto-parietal region and the patient's condition deteriorated (Fig. 1B). The tumor was removed again and a fresh tumor specimen was obtained in the operating room through the cryostat laboratory. The patient relapsed with leptomeningeal seeding 2 months after the surgery and subsequently passed away, despite a series of additional surgery, chemotherapy and radiation therapy. The patient diagnosed with GBM was a 61-year-old male, who was presented with tingling sensation in the left hand and twitching in the left arm and face. MRI showed a 3.5-cm-sized enhanced mass in the right parietal lobe. The patient underwent total removal of the tumor. Pathology showed GBM and the patient underwent concurrent chemoradiation therapy as well as a series of chemotherapy (temozolomide). Chemotherapy was reinitiated after radiological evidence of tumor recurrence.

Isolation and culture of rPB TSs. A surgical specimen from the rPB patient was freshly obtained from the operating room. Informed consent was provided according to the Declaration of Helsinki. Neuropathologists diagnosed each surgical specimen according to the WHO classification criteria (19). TSs were isolated from the rPB specimen using a modification of previous methods for TS isolation from human brain cancers (11,13,15,20,21). Briefly, the cell isolation procedure was performed within 60 min of PB removal using a mechanical dissociation method. The surgical specimen was minced and dissociated with a scalpel in Dulbecco's modified Eagle's medium/Nutrient Mixture F-12 (DMEM/F-12; Mediatech, Manassas, VA, USA) and then passed through a series of 100-μm nylon mesh cell strainers (BD Falcon; BD Biosciences Franklin Lakes, NJ, USA). Cell suspensions were washed twice in DMEM/F-12 and cultured in complete TS media composed of DMEM/F-12 containing B27 supplements (1X; Invitrogen, San Diego, CA, USA), 20 ng/ml of basic fibroblast growth factor (bFGF; Sigma, St. Louis, MO, USA), 20 ng/ml of epidermal growth factor (EGF; Sigma), and 50 U/ml penicillin/50 mg/ml streptomycin (11,22-25). In addition, glioblastoma (GBM) TSs (TS13-20), isolated from a primary GBM patient, were used for comparison with rPB TSs.

Immunocytochemical staining. For investigation of surface and intracellular antigen expression profiles, rPB TSs were transferred to cover slides, fixed with 2% paraformaldehyde for 7 min, and then treated with a 3:1 ratio of methanol and

acetic acid for 3 min. The cells were then washed and permeabilized by incubating with 0.1% Triton X-100 for 10 min. After blocking with 1% bovine serum albumin (BSA; Amresco, Solon, OH, USA) for 1 h, cells were incubated with primary antibodies for 2 h at room temperature. The following antibodies were used: rabbit anti-CD133 (1:250, ab19898; Abcam Dawinbio Inc., Hanam, Korea), rabbit anti-musashi (1:250, ab52865; Abcam) and rabbit anti-podoplanin (1:250, ab10274; Abcam). Primary antibody against CD133 was detected with goat anti-rabbit IgG conjugated with Alexa Fluor 555 (1:2,000; Invitrogen), which is spectrally similar to Cy3. Alexa Fluor 488-conjugated goat anti-rabbit IgG (1:2,000; Invitrogen) was used to detect antibodies against musashi and podoplanin. The cells were mounted with Vectashield H-1200 mounting media containing 4'6-diamidino-2-phenylindole (DAPI; Vector Laboratories, Burlingame, CA, USA) to counterstain nuclei. Phosphate-buffered saline (PBS; Dawinbio Inc., Hanam, Korea) was used for all washing steps, and antibody diluent reagent solution (Invitrogen) was used to dilute antibodies. As a negative control, only the secondary antibody was used. A fluorescence microscope (1X71; Olympus Korea, Co., Ltd., Seoul, Korea) and DP Controller software (Olympus Korea) were used for observing and photographing the cells.

Reverse-transcription polymerase chain reaction (RT-PCR). Total RNA was isolated from rPB TSs (TS13-19) and GBM TSs (TS13-20) using an RNeasy kit (Qiagen, Hilden, Germany). cDNA was synthesized from 2 μg of total RNA using the SuperScript II First-Strand Synthesis system (Invitrogen). The following oligonucleotide primer pairs were used for PCR: GAPDH (glyceraldehyde-3-phosphate dehydrogenase), 5'-AGG GGT CTA CAT GGC AAC TG-3' and 5'-ACC CAG AAG ACT GTG GAT GG-3'; CD133, 5'-GCC AGC CTC AGA CAG AAA AC-3' and 5'-TAC CTG GTG ATT TGC CAC AA-3'; podoplanin, 5'-CCA GCG AAG ACC GCT ATA AB-3' and 5'-AGA GGA GCC AAG TCT GGT GA-3'; musashi-1, 5'-ACC CCC ACA TTC TCT CAC TG-3' and 5'-GAG ACA CCG GAG GAT GGT AA-3'; GFAP (glial fibrillary acidic protein), 5'-AGA TCC ACG AGG AGG AGG TT-3' and 5'-CGG CGT TCC ATT TAC AAT CT-3'; Olig2 (oligodendrocyte transcription factor 2), 5'-CAG AAG CGC TGA TGG TCA TA-3' and 5'-AAGGGTGTTACACGGCAGAC-3'; TUBB3 (β-tubulin III), 5'-CAT CCA GAG CAA GAA CAG CA-3' and 5'-GCC TGG AGC TGC AAT AAG AC-3'; β-catenin, 5'-GCT TGG TTC ACC AGT GGA TT-3' and 5'-GAG TCC CAA GGA GAC CTT CC-3'; snail, 5'-GAG CAT ACA GCC CCA TCA CT-3' and 5'-TTG GAG CAG TTT TTG CAC TG-3'; Zeb1 (zinc finger E-box binding homeobox 1), 5'-GAC AGG GCT GAA AGT AGT CAA GC-3' and 5'-GGT AGT TAG CAC GGG TTG GA-3'.

Quantitative real-time PCR. Total RNA from rPB TSs was prepared using an RNeasy kit (Qiagen) and reverse transcribed using a First-Strand cDNA Synthesis kit (Invitrogen) according to the manufacturer's instructions. Changes in expression levels were quantitatively analyzed using a real-time PCR machine (StepOne Plus; Applied Biosystems, Foster City, CA, USA). Specific commercial TaqMan probes (Applied Biosystems) were used to quantify levels of the following mRNAs: CD133, podoplanin, nestin, musashi-1, Sox2, Oct4, β-catenin, snail and Zeb1. For analysis of relative gene expression, rPB TSs were tested in triplicate; transcript levels of GBM TSs were monitored as an internal control.

Neuro-glial differentiation. The multipotency of rPB TSs was tested by examining neural lineage expression by immunocytochemical staining, as previously described (11,20,26). Briefly, after being seeded onto chamber slides (Lab-Tek II; Nalge Nunc International, Rochester, NY, USA), cells were grown in neural differentiation media containing 10% fetal bovine serum (FBS; Lonza) and 1X B27 supplement (Invitrogen) for up to 14 days. Cells were then fixed with 2% paraformaldehyde for 7 min at 4˚C, and permeabilized by incubating with 0.1% Triton X-100 for 10 min. After blocking with 1% BSA (Amresco) for 1 h, cells were immunostained with the following antibodies: rabbit anti-GFAP (1:200 dilution; Dako, Carpinteria, CA, USA), mouse anti-MBP (myelin basic protein, 1:200 dilution; Chemicon International, Inc., Temecula, CA, USA), mouse anti-NeuN (1:100 dilution; Chemicon) and mouse anti-TUBB3 (Tuj1, 1:200 dilution; Chemicon). The primary antibodies were detected with Cy3-conjugated anti-mouse or anti-rabbit secondary antibodies (1:200 dilution; Jackson ImmunoResearch Laboratories, West Grove, PA, USA), as appropriate. Nuclei were counterstained with DAPI (Vector Laboratories). Slides were examined and photographed using a fluorescence microscope.

Three-dimensional (3D) invasion assay. For invasion assays, collagen I/Matrigel matrices were prepared from 2.4 mg/ml of high-concentration rat tail collagen type I (Corning Life Sciences, Tewksbury, MA, USA), 2.1 mg/ml of Matrigel (Corning Life Sciences), 10% $NaHCO_3$ and 2X TS culture medium. The solution was well mixed and kept at 4˚C before use. Single rPB TSs and GBM TSs were each placed individually onto 100 μl collagen I/Matrigel matrices in a 96-well plate and plates were incubated at 37.4˚C in a 5% CO_2 environment for 30 min. After full gelation of the matrix, 100 μl of TS culture medium was added on top. The dynamic morphology of rPB TSs and GBM TSs was observed by collecting images using an inverted microscope (Optinity KI 400; Intron Biotechnology, Inc., Seongnam, Korea). For quantification, the maximal area covered by migrating edges of cells was used as the parameter for defining invasiveness, calculated as the invaded area at a certain time/spheroid area at initial time x 100. Data were analyzed using ToupView image analysis software (x64 v3.7.1460; AmScope, Irvine, CA, USA).

Orthotopic rPB TS xenograft. Four-to 8-week-old male athymic nude mice (Central Lab. Animal Inc., Seoul, Korea) were used for experiments. Mice were housed in micro-isolator cages under sterile conditions and observed for at least 1 week before study initiation to ensure proper health. Lighting, temperature and humidity were controlled centrally. All experimental procedures were approved by the Yonsei University College of Medicine Institutional Animal Care and Use Committee. Mice were anesthetized with a solution of Zoletil (30 mg/kg; Virbac Korea, Co., Ltd., Seoul, Korea) and xylazine (10 mg/kg; Bayer Korea, Seoul, Korea), delivered intraperitoneally. rPB TSs were implanted into the right frontal lobe of nude mice using a guide-screw system within the skull, as previously

described (22,24,25,27-29). Mice received $5x10^5$ rPB TSs via a Hamilton syringe (Dongwoo Science, Co., Seoul, Korea), inserted to a depth of 4.5 mm. rPB TSs were injected into three mice simultaneously using a multiple micro-infusion syringe pump (Harvard Apparatus, Holliston, MA, USA) at a speed of 0.5 μl/min. Body weights of mice were checked every other day. If body weight decreased by >15% compared to the original weight, mice were euthanized according to the study protocol. Formalin-fixed, paraffin-embedded tissue blocks were used for the generation of slides for histologic examination. Hematoxylin and eosin (H&E)-stained sections were reviewed by a pathologist.

DNA extraction and forensic short tandem repeat (STR) typing. DNA was extracted from paraffin embedded tissues and their stem cells using a QIAamp DNA Mini kit (Qiagen) according to the manufacturer's instructions. DNA extracted from reference tissues and stem cells was measured using a NanoDrop 1000 Spectrophotometer (Thermo Fisher Scientific, Waltham, MA, USA) and diluted to 1 ng/μl. For specific detection of human DNA in xenografts extracted from mouse tissue, DNA was quantified using a Quantifiler Duo DNA Quantification kit (Applied Biosystems), according to the manufacturer's instructions. The DNA quantity ranged from 42 to 126 pg/μl. Extracted DNA was tested for the genotypes of amelogenin and 23 forensic STRs (D3S1358, D1S1656, D2S441, D10S1248, D13S317, D16S539, D18S51, D2S1338, CSF1PO, TH01, vWA, D21S11, D7S820, D5S818, TPOX, D8S1179, D12S391, D19S433, FGA, D22S1045, Penta E, Penta D and DYS391). PCR amplification using PowerPlex Fusion (Promega Corp., Madison, MI, USA), Kplex-16 (BioQuest, Inc., Seoul, Korea) and Euplex-13 (BioQuest), performed according to the manufacturer's instruction using 1 ng of DNA extracted from human tissue and stem cells, were used to maximize STR genotypes obtained from degraded DNA in paraffin-embedded tissue. DNA extracted from mouse tissue was amplified by PCR essentially as described by the manufacturer, except that 5 μl of the extracted DNA was used and two additional PCR cycles were performed to increase the PCR yield of each multiplex system. All PCR amplifications were performed in duplicate in two additional independent experiments. PCR products were separated by capillary electrophoresis using an ABI PRISM 3130xl Genetic Analyzer (Applied Biosystems), and the results were analyzed using GeneMapper ID Software version 3.2 (Applied Biosystems). The genotypes of amelogenin and STRs were determined based on observation of each allele at least two additional times in independent tests.

Gene expression microarray analysis and gene set enrichment analysis. Total RNA was extracted from rPB-TSs and 4 GBM-TSs that were established using a Qiagen miRNA kit according to the manufacturer's protocol. Expression profiles of TSs from rPB and GBM (control) were obtained using an Illumina HumanHT-12 v4 Expression BeadChip (Illumina, Inc., San Diego, CA, USA). Data were variance stabilizing transformed and normalized with the quantile normalization method using R/Bioconductor lumi package. Complete linkage hierarchical clustering with distance metric by taking distance = (1-corelation)/2, was performed and depicted as heatmap. Comparative Marker Viewer version 7.13 of GenePattern

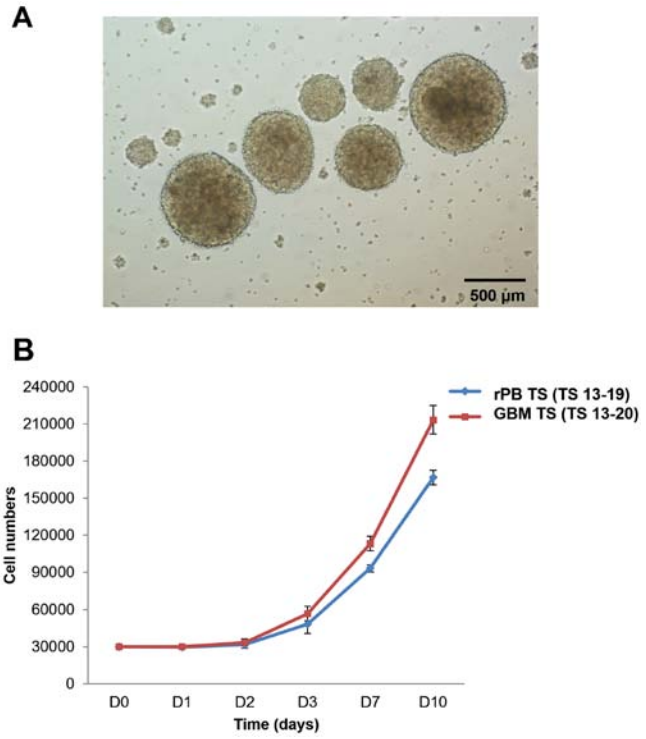

Figure 2. Morphology and growth curve of rPB TSs (TS 13-19). (A) Morphology of TSs formed using single cells from surgically removed PB tissue shown by phase-contrast microscopy (original magnification, x100). (B) Growth curves of rPB TSs and GBM TSs (TS 13-20) based on cell counts on days 1, 2, 3, 7 and 10. Data are presented means ± SD.

module was used for differential expression of two groups. Gene set enrichment analysis was performed using gene sets of hallmark signatures and those composed of genes upregulated in metastasis and epithelial mesenchymal transition, all of them provided by the Molecular Signatures Database (v5.0 MSigDB) (30).

Statistical analysis. Data are expressed as means ± standard deviations. Comparisons between two groups were done using the Student's t-test. P-values <0.05 or false discovery rate <25% were considered statistically significant.

Results

Morphology and growth characteristics of rPB TSs. Cells isolated from the rPB specimen yielded spheroids when cultured in TS complete media (Fig. 2A). These spheroids (TS 13-19), termed rPB TSs, proliferated ~5- to 6-fold in 10 days. This proliferation pattern was similar to that of GBM TSs (TS 13-20), which grew ~7-fold in 10 days (Fig. 2B).

Stemness of rPB TSs. To examine the stemness of rPB TSs, we used neurosphere formation assays, immunocytochemical staining and RT-PCR and qPCR analyses. Results from these studies were compared with those for GBM TSs. Neurosphere assays confirmed the presence of cells with extensive self-renewal ability in the rPB specimen. The size of neurospheres increased over time for both rPB TSs and GBM TSs (Fig. 3A), as could be seen grossly by light microscopy and as quantified by sphere radius measurements on days 3, 7 and 10.

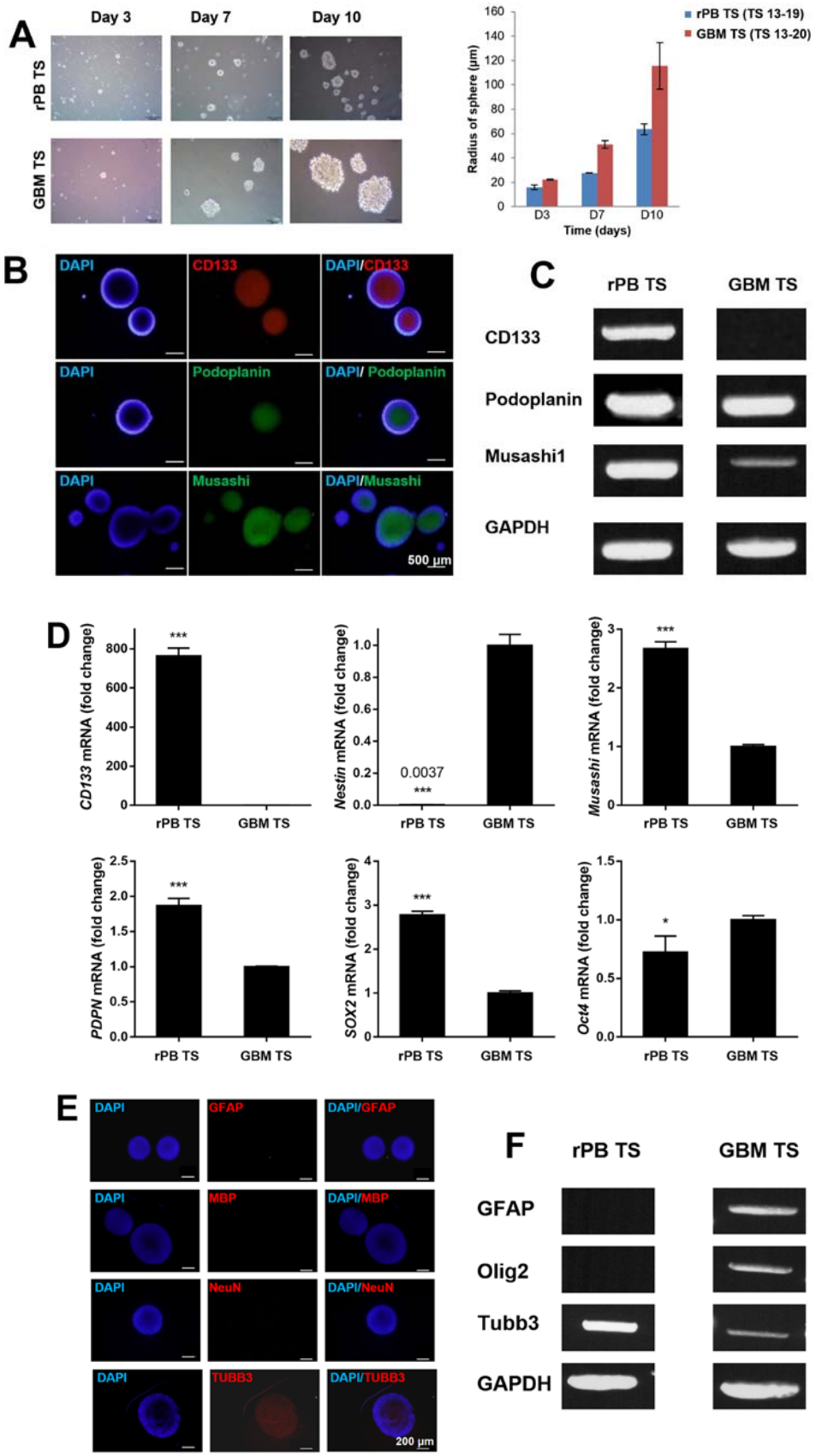

Figure 3. Stemness and differentiation potential of rPB TSs characterized by neurosphere formation, immunocytochemical staining, RT-PCR and qPCR. (A) *In vitro* formation of TSs from single rPB TS cells (original magnification, x100) and GBM TS cells on days 3, 7 and 10. The bar graph compares the radii of rPB TSs with those of GBM TSs on days 3, 7 and 10. (B) Immunocytochemical staining of rPB TS cells for CD133, podoplanin and musashi; nuclei were counterstained with DAPI (original magnification, x100). (C) RT-PCR analysis of rPB TSs and GBM TSs for CD133, podoplanin and musashi. GAPDH was used as a control. (D) qPCR analysis of rPB TSs and GBM TSs for CD133, podoplanin, nestin, musashi, Sox2 and Oct4. Each sample was analyzed in triplicate. *P<0.05, ***P<0.001, n=3 for Student's t-test. (E) Immunocytochemical staining against GFAP, MBP, NeuN and TUBB3 from rPB TSs grown in neural differential media (original magnification, x200). (F) RT-PCR analysis for selected differentiation markers including GFAP, Olig2 and TUBB3 from rPB TSs and GBM TSs grown in neural differential media. GAPDH was used as a control. Each sample was analyzed in triplicate. *P<0.05.

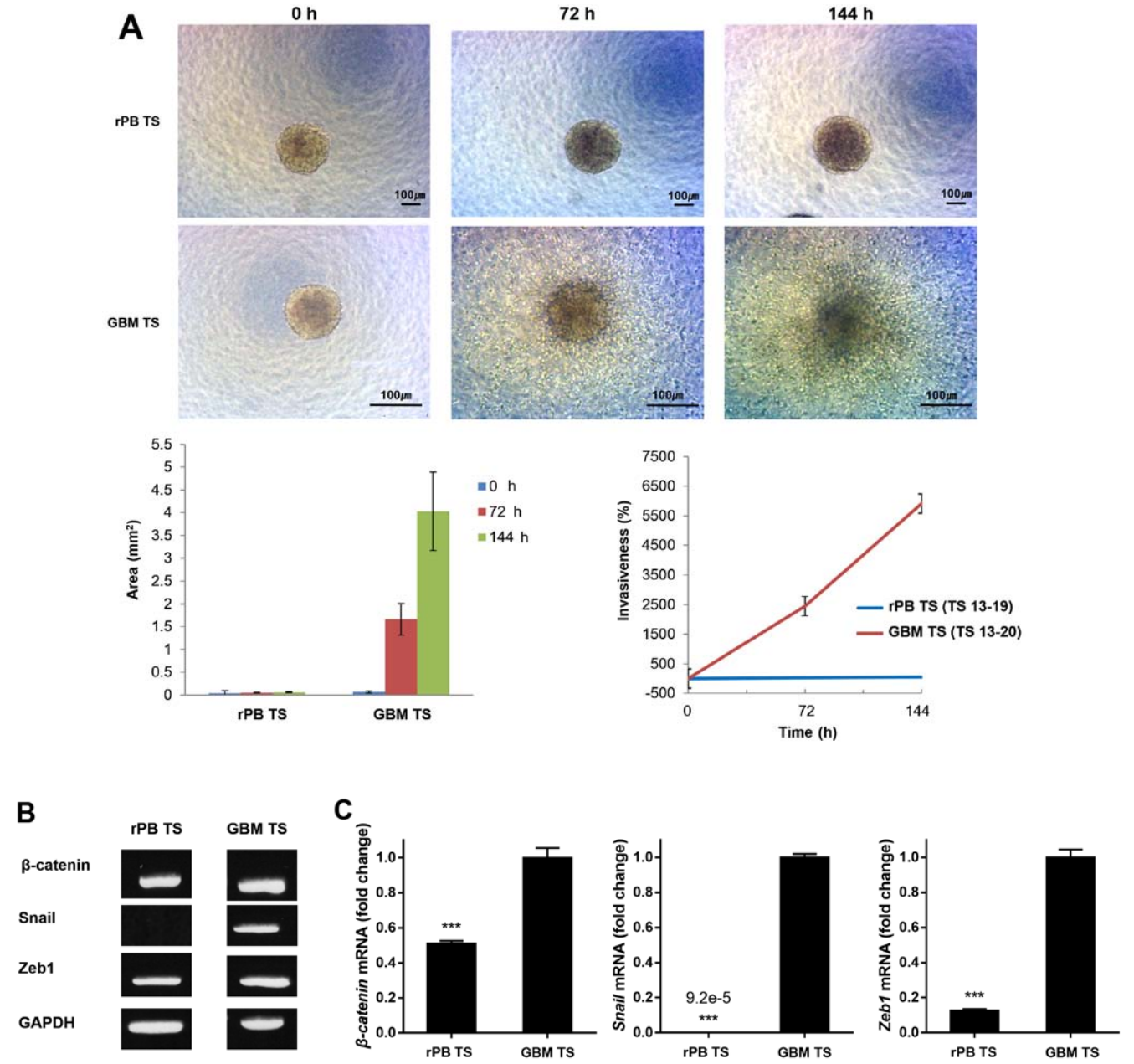

Figure 4. Comparison of rPB TSs and GBM TSs invasiveness. (A) 3D invasion assay (original magnification, x200) and TS area at 0, 72 and 144 h. Area and invasiveness of rPB TSs at three time-points compared with those of GBM TSs. Maximal area covered by migrating edges of cells was used as a parameter for defining invasiveness, calculated as invaded area at a certain time/spheroid area at initial time x 100. (B) RT-PCR analysis for selected invasion markers, including β-catenin, snail and Zeb1. GAPDH was used as a control. (C) qPCR analysis for selected invasion markers, including β-catenin, snail and Zeb1. Each sample was analyzed in triplicate. ***P<0.001, n=3 for Student's t-test.

Immunocytochemical staining of rPB TSs identified cells expressing markers associated with stem cells and brain tumor stem cells (31), including CD133, podoplanin and musashi (Fig. 3B). To further assess the stemness of rPB TSs at the gene level, we used RT-PCR and qPCR analyses to measure CD133, podoplanin, nestin, musashi, Sox2 and Oct4 expression levels. Whereas both rPB TSs and GBM TSs expressed all stem cell surface markers, expression of CD133, podoplanin, musashi and Sox2 was significantly higher in rPB TSs (Fig. 3C and D), whereas expression of nestin and Oct4 was higher in GBM TSs.

Neuro-glial differentiation of rPB TSs. To assess the multilineage differentiation capacity of rPB TSs, we cultured them in neuro-glial differentiation media as described in Materials and methods. Immunocytochemical staining with Tujl demonstrated that rPB TSs expressed TUBB3, a marker for immature neurons; however, they did not express other differentiation markers such as GFAP, MBP, or NeuN, which are specific for astrocytes, oligodendrocytes and mature neurons, respectively (Fig. 3E). RT-PCR analyses showed that rPB TSs expressed higher level of TUBB3, but lower levels of GFAP and Olig2 compared with GBM TSs (Fig. 3F). These results make sense given that pineocytes are specialized neurons (32), and give rise to tumors that are distinct from tumors of glial origin, such as GBMs, which express surface markers for oligodendrocytes, astrocytes and mature and immature neurons.

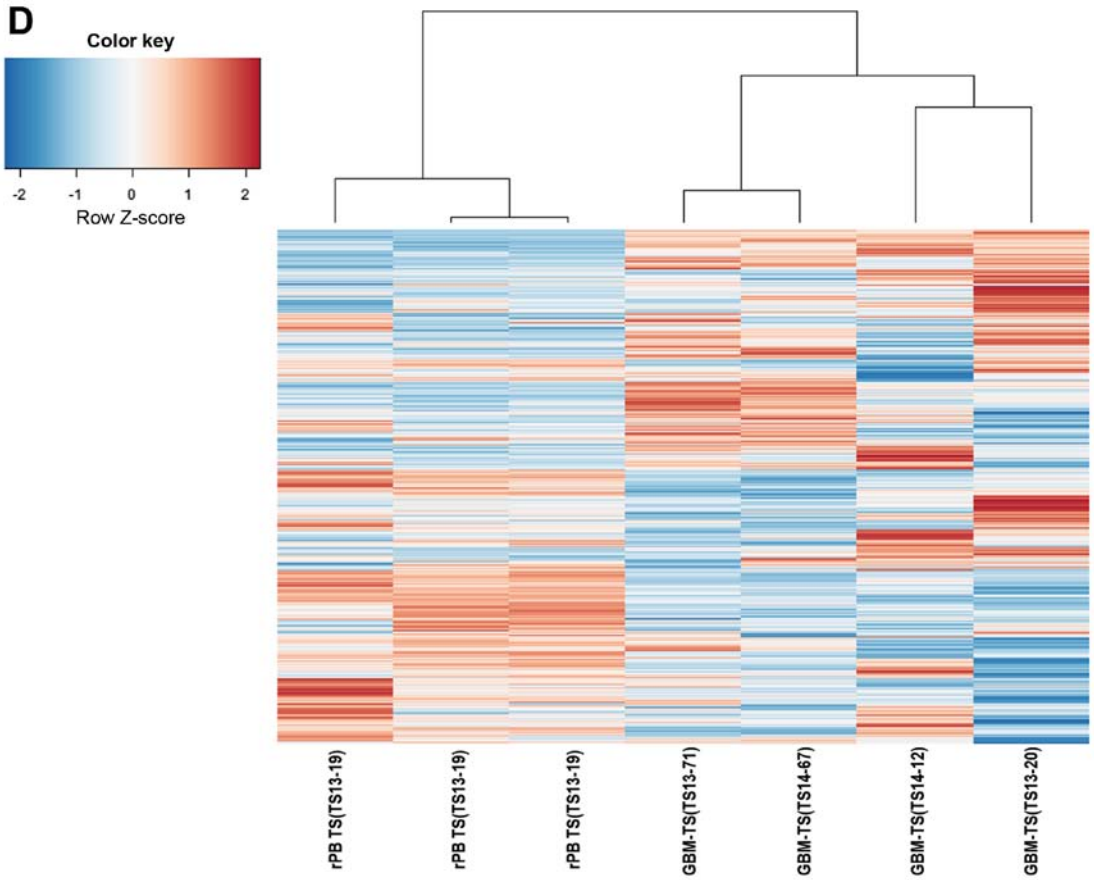

Figure 4. Continued. (D) Hierarchical cluster map of the whole genes for rPB TSs and GBM TSs. Sets of genes of rPB TSs are differentially expressed from those of GBMs.

Invasiveness of rPB TSs. rPB TSs invasion patterns were investigated using 3D invasion assays. Light microscopy showed no overt evidence for invasion by rPB TSs at 0, 72 or 144 h, whereas GBM TSs were clearly invasive at 72 and 144 h (Fig. 4A). From 0 to 144 h, the area occupied by rPB TSs increased ~1.2-fold, whereas that of GBM TSs increased by 63.7-fold. At 144 h, the areas were significantly different between the groups ($P<0.05$). The relative invasiveness, calculated by comparing maximal areas, was 43% for rPB TSs and 5911% for GBM TSs ($P<0.005$). An RT-PCR analysis of epithelial-mesenchymal transition (EMT) markers detected expression of β-catenin and Zeb1 in rPB TSs and GBM TSs, and additionally detected snail in GBM TSs (Fig. 4B). A qPCR analysis found that all three EMT genes were expressed in both rPB TSs and GBM TSs, but were expressed at significantly lower levels in rPB TSs (Fig. 4C).

Gene expression profile of rPB TSs compared with GBM TSs and gene set enrichment analysis. To assess the difference in the expression of genes between rPB TSs and GBM TSs, we performed whole-genome expression profiling. rPB TSs showed a gene expression profile distinct from that of GBM TSs of different origin, as depicted in the heatmap shown in Fig. 4D. Differential expression analysis revealed 4809 genes with false discovery rate <25%. Highly ranked genes in the comparative marker selection analysis included ARID3B, NOP56, RPOS4Y1 and JARID2, all of which were known to be expressed in embryonal tumors or cell lines derived from them. Gene set enrichment analysis revealed the activation of myc-targeted genes in rPB TSs with statistical significance whereas gene sets upregulated in metastasis and epithelial mesenchymal transition were activated in GBM TS.

Establishment of orthotopic mouse model from patient-derived rPB TSs. To determine the tumorigenic potential of rPB TSs, we injected them into the right cerebrum of male athymic nude mice. Mice were euthanized when their weight decreased by >15% relative to their original body weight. A cross-sectional slice showed the presence of an intracerebral xenograft tumor (Fig. 5A, right image). To determine whether the xenograft tumor replicated phenotypes of the parent tumor, we compared histological features of xenograft tumors with those of the parent tumor tissue obtained in the initial surgery (Fig. 5A, right image, corresponding to the tumor in Fig. 1A) and from surgery after recurrence (Fig. 5A, middle image, corresponding to the tumor in Fig. 1B). A pathologist confirmed that histopathological findings of all three tissues showed common characteristics of embryonal tumors, including high cellularity, increased mitotic index and high nucleus-cytoplasm ratio. A test of the genotypes of amelogenin and 23 forensic STRs (D3S1358, D1S1656, D2S441, D10S1248, D13S317, D16S539, D18S51, D2S1338, CSF1PO, TH01, vWA, D21S11, D7S820, D5S818, TPOX, D8S1179, D12S391, D19S433, FGA, D22S1045, Penta E, Penta D and DYS391) showed that all autosomal STR profiles were identical, indicating that the

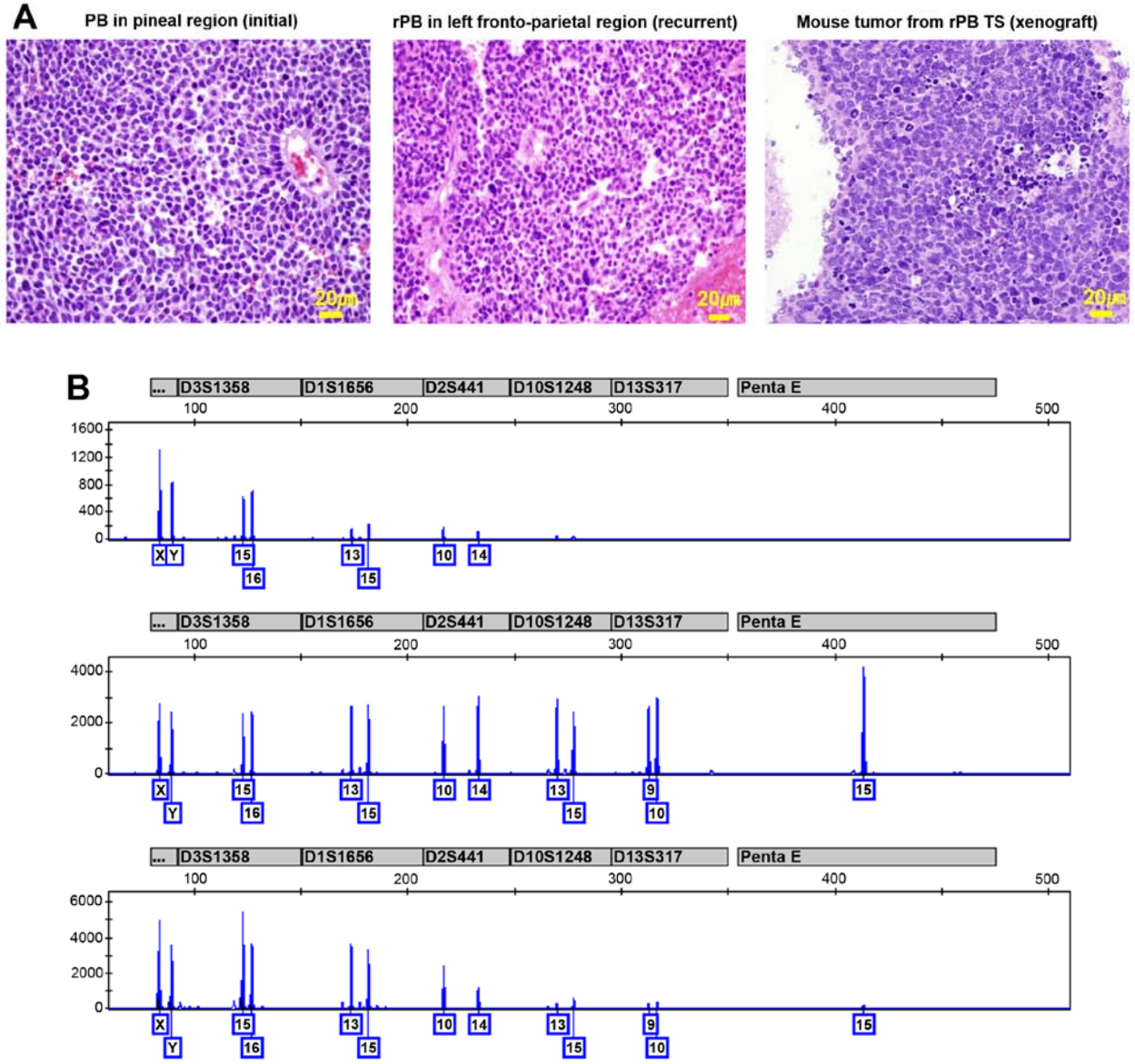

Figure 5. Histological and genetic characterization of the rPB TS orthotopic mouse model. (A) Comparison of PB tissue from the patient and the orthotopic mouse model. H&E staining showing the histology of the PB at initial surgery (left) and at recurrence (middle), and the xenograft tumor (right). (B) Genomic profiles (STRs) of the three PB tissues.

genomic alterations found in the parental rPB were replicated in the corresponding xenograft tumors (Fig. 5B).

Discussion

In the present study, we describe the first report of the isolation of TSs from an rPB specimen. We confirmed that the rPB TS cells have strong self-renewal and tumor-initiating capacity, while lacking the ability for multi-lineage differentiation typical of GBM TSs. In addition, 3D invasion and gene expression studies showed that rPB TSs are not as invasive as GBM TSs. An orthotopic xenograft model created using rPB TSs replicated the parent tumor histopathologically as well as genetically, supporting the potential use of rPB TSs for patient-derived xenograft (PDX) models of PB.

The invasive behavior of rPB TSs and GBM TSs was different, with rPB TSs showing no overt evidence of invasion in 3D invasion assays and GBM TSs, demonstrating a clear invasive pattern (Fig. 4A). These features correlate with the characteristic invasive patterns of the two tumors as observed in MRI. PBs feature a well-circumscribed (33,34), lobulated, and solid lesion with avid contrast enhancement (35), as evident in MRIs of both the patient's original and recurred PB (Fig. 1B). In contrast, GBMs are highly infiltrative and have irregular borders; their mass infiltrates the brain parenchyma via white matter tracks (Fig. 1C) (36), thereby increasing the isotropic component in diffusion tensor imaging (DTI) (37). Some studies have shown that PBs can invade the surrounding brain parenchyma (38,39) and may disseminate through the cerebrospinal fluid (40,41). However, we were unable to find many studies showing radiologically infiltrative PBs, suggesting that PBs with invasiveness comparable to that of GBMs are rare. Such a low degree of invasiveness of rPB TSs compared with GBM TSs might result from the lower expression levels of EMT-associated genes in rPB TSs (Fig. 4B and C). In many different cancers, a number of transcription factors, including

snail, slug, Zeb1 and twist, have been identified as important EMT regulators (42). Studies have also shown that β-catenin, a downstream target of AKT, is capable of modulating the aggressive phenotype of cancer cells (42,43). Compared with GBM TSs, the levels of EMT genes, including β-catenin, snail and Zeb1, were all significantly lower in rPB TSs (Fig. 4B). In particular, the greater invasiveness of GBM TSs compared with rPB TSs demonstrated by our data might be attributable to the high expression level of snail, which is known to be at least ten times more potent than Zeb1 in repressing standard epithelial markers, such as E-cadherin and Mucin-1 (44).

Examples of xenograft models that have been created to recapitulate human glioma in animals include: i) xenografts based on human glioma-derived cell lines passaged in neurobasal medium; ii) biopsy spheroid xenograft models or PDX; and iii) human glioma monolayer cell lines established in serum-containing media (45). Our xenograft model is conceptually in line with the first approach. One advantage of this approach lies in the ease of propagating TSs to yield sufficient material for potential biomarker and therapeutics discovery, while recapitulating the histology of the patient tumor (45). While it is true that this approach might allow clonal selection to take place during passage, thereby changing the genetic and epigenetic information, the results of our genetic studies show that such selection did not take place in the xenograft model. By establishing an orthotopic mouse model from patient-derived rPB TSs, we have provided the first demonstration of the feasibility of creating a PDX model using TSs from rPB. Although we did not use mutational status, DNA copy number variation, or gene expression to evaluate the genetic correlation between our xenograft model and the original tumor as have some previous reports on PDX (46), we believe that our data (Fig. 5A and B) provide sufficient histological and genetic evidence to demonstrate the identity of the orthotopic xenograft model with the parent tumor. In this regard, we suggest that our mouse orthotopic xenograft model of rPB TSs represents an alternative method for establishing a PDX.

Studies have shown that biopsy spheroid xenograft models, or PDXs, can well replicate the invasive characteristics and other histological features of the original patient tumor, including human-derived microvasculature, host extracellular matrix and resident macrophages (45,47). However, one major disadvantage of this model is time; it can take 2-11 months for the initial engraftment and an additional 8-18 months for the minimum of three passages required to develop xenografts that resemble the parent tumor (45,48). Another potential difficulty presented by the genetic heterogeneity of PDXs might be standardization of the model. Notwithstanding these potential limitations, we believe that our xenograft model using rPB TSs is not only efficient, but also more effective in establishing a standardized *in vivo* model of PBs that is genetically indistinguishable from the patient tumor. In the future, incorporating genome sequencing, proteomics and metabolomics would improve this platform for use in studying cancer stem-cell biology and developing novel cancer therapeutics (46).

Acknowledgements

We thank Dr Hyun-Jung Kee, Department of Surgery, Yonsei University College of Medicine, Seoul, Korea, for providing help with array experiments. The present study was supported by a faculty research grant from the Yonsei University College of Medicine for 2013 (6-2013-0034), and by grants from the Basic Science Research Program through the National Research Foundation of Korea (NRF) funded by the Ministry of Education, Science and Technology (NRF-2013R1A1A2006427), and the Korean Health Technology R&D Project, Ministry of Health & Welfare, Republic of Korea (HI13C1509).

References

1. Lutterbach J, Fauchon F, Schild SE, Chang SM, Pagenstecher A, Volk B, Ostertag C, Momm F and Jouvet A: Malignant pineal parenchymal tumors in adult patients: patterns of care and prognostic factors. Neurosurgery 51: 44-55; discussion 55-46, 2002.
2. Kobayashi T and Lunsford L: Pineal Region Tumors, Diagnosis and Treatment Options. Karger, Pittsburgh, PA, 2009.
3. Friedrich C, von Bueren AO, von Hoff K, Gerber NU, Ottensmeier H, Deinlein F, Benesch M, Kwiecien R, Pietsch T, Warmuth-Metz M, *et al*: Treatment of young children with CNS-primitive neuroectodermal tumors/pineoblastomas in the prospective multicenter trial HIT 2000 using different chemotherapy regimens and radiotherapy. Neuro Oncol 15: 224-234, 2013.
4. Schild SE, Scheithauer BW, Schomberg PJ, Hook CC, Kelly PJ, Frick L, Robinow JS and Buskirk SJ: Pineal parenchymal tumors. Clinical, pathologic, and therapeutic aspects. Cancer 72: 870-880, 1993.
5. Lee JY, Wakabayashi T and Yoshida J: Management and survival of pineoblastoma: an analysis of 34 adults from the brain tumor registry of Japan. Neurol Med Chir (Tokyo) 45: 132-141; discussion 141-132, 2005.
6. Miller S, Rogers HA, Lyon P, Rand V, Adamowicz-Brice M, Clifford SC, Hayden JT, Dyer S, Pfister S, Korshunov A, *et al*: Genome-wide molecular characterization of central nervous system primitive neuroectodermal tumor and pineoblastoma. Neuro Oncol 13: 866-879, 2011.
7. Dean M, Fojo T and Bates S: Tumour stem cells and drug resistance. Nat Rev Cancer 5: 275-284, 2005.
8. Huntly BJ and Gilliland DG: Leukaemia stem cells and the evolution of cancer-stem-cell research. Nat Rev Cancer 5: 311-321, 2005.
9. Visvader JE and Lindeman GJ: Cancer stem cells in solid tumours: Accumulating evidence and unresolved questions. Nat Rev Cancer 8: 755-768, 2008.
10. Singh SK, Hawkins C, Clarke ID, Squire JA, Bayani J, Hide T, Henkelman RM, Cusimano MD and Dirks PB: Identification of human brain tumour initiating cells. Nature 432: 396-401, 2004.
11. Kong BH, Park NR, Shim JK, Kim BK, Shin HJ, Lee JH, Huh YM, Lee SJ, Kim SH, Kim EH, *et al*: Isolation of glioma cancer stem cells in relation to histological grades in glioma specimens. Childs Nerv Syst 29: 217-229, 2013.
12. Hussein D, Punjaruk W, Storer LC, Shaw L, Othman RT, Peet A, Miller S, Bandopadhyay G, Heath R, Kumari R, *et al*: Pediatric brain tumor cancer stem cells: Cell cycle dynamics, DNA repair, and etoposide extrusion. Neuro Oncol 13: 70-83, 2011.
13. Singh SK, Clarke ID, Terasaki M, Bonn VE, Hawkins C, Squire J and Dirks PB: Identification of a cancer stem cell in human brain tumors. Cancer Res 63: 5821-5828, 2003.
14. Sutter R, Shakhova O, Bhagat H, Behesti H, Sutter C, Penkar S, Santuccione A, Bernays R, Heppner FL, Schüller U, *et al*: Cerebellar stem cells act as medulloblastoma-initiating cells in a mouse model and a neural stem cell signature characterizes a subset of human medulloblastomas. Oncogene 29: 1845-1856, 2010.
15. Sulman E, Aldape K and Colman H: Brain tumor stem cells. Curr Probl Cancer 32: 124-142, 2008.
16. Gupta PB, Onder TT, Jiang G, Tao K, Kuperwasser C, Weinberg RA and Lander ES: Identification of selective inhibitors of cancer stem cells by high-throughput screening. Cell 138: 645-659, 2009.
17. Nautiyal J, Kanwar SS, Yu Y and Majumdar AP: Combination of dasatinib and curcumin eliminates chemo-resistant colon cancer cells. J Mol Signal 6: 7, 2011.

18. Hermann PC, Huber SL, Herrler T, Aicher A, Ellwart JW, Guba M, Bruns CJ and Heeschen C: Distinct populations of cancer stem cells determine tumor growth and metastatic activity in human pancreatic cancer. Cell Stem Cell 1: 313-323, 2007.
19. Louis DN, Ohgaki H, Wiestler OD, Cavenee WK, Burger PC, Jouvet A, Scheithauer BW and Kleihues P: The 2007 WHO classification of tumours of the central nervous system. Acta Neuropathol 114: 97-109, 2007.
20. Kwak J, Shin HJ, Kim SH, Shim JK, Lee JH, Huh YM, Kim EH, Park EK, Chang JH, Kim SH, *et al*: Isolation of tumor spheres and mesenchymal stem-like cells from a single primitive neuroectodermal tumor specimen. Childs Nerv Syst 29: 2229-2239, 2013.
21. Kim SM, Kang SG, Park NR, Mok HS, Huh YM, Lee SJ, Jeun SS, Hong YK, Park CK and Lang FF: Presence of glioma stroma mesenchymal stem cells in a murine orthotopic glioma model. Childs Nerv Syst 27: 911-922, 2011.
22. Kang SG, Cheong JH, Huh YM, Kim EH, Kim SH and Chang JH: Potential use of glioblastoma tumorsphere: Clinical credentialing. Arch Pharm Res 38: 402-407, 2015.
23. Kong BH, Moon JH, Huh YM, Shim JK, Lee JH, Kim EH, Chang JH, Kim DS, Hong YK, Kim SH, *et al*: Prognostic value of glioma cancer stem cell isolation in survival of primary glioblastoma patients. Stem Cells Int 838950: 2014, 2014.
24. Kong BH, Shin HD, Kim SH, Mok HS, Shim JK, Lee JH, Shin HJ, Huh YM, Kim EH, Park EK, *et al*: Increased *in vivo* angiogenic effect of glioma stromal mesenchymal stem-like cells on glioma cancer stem cells from patients with glioblastoma. Int J Oncol 42: 1754-1762, 2013.
25. Shin GY, Shim JK, Lee JH, Shin HJ, Lee SJ, Huh YM, Kim EH, Park EK, Kim SH, Chang JH, *et al*: Changes in the biological characteristics of glioma cancer stem cells after serial in vivo subtransplantation. Childs Nerv Syst 29: 55-64, 2013.
26. Kim YG, Jeon S, Sin GY, Shim JK, Kim BK, Shin HJ, Lee JH, Huh YM, Lee SJ, Kim EH, *et al*: Existence of glioma stroma mesenchymal stemlike cells in Korean glioma specimens. Childs Nerv Syst 29: 549-563, 2013.
27. Lal S, Lacroix M, Tofilon P, Fuller GN, Sawaya R and Lang FF: An implantable guide-screw system for brain tumor studies in small animals. J Neurosurg 92: 326-333, 2000.
28. Lim HY, Kim KM, Kim BK, Shim JK, Lee JH, Huh YM, Kim SH, Kim EH, Park EK, Shim KW, *et al*: Isolation of mesenchymal stem-like cells in meningioma specimens. Int J Oncol 43: 1260-1268, 2013.
29. Kang SG, Shinojima N, Hossain A, Gumin J, Yong RL, Colman H, Marini F, Andreeff M and Lang FF: Isolation and perivascular localization of mesenchymal stem cells from mouse brain. Neurosurgery 67: 711-720, 2010.
30. Subramanian A, Tamayo P, Mootha VK, Mukherjee S, Ebert BL, Gillette MA, Paulovich A, Pomeroy SL, Golub TR, Lander ES, *et al*: Gene set enrichment analysis: A knowledge-based approach for interpreting genome-wide expression profiles. Proc Natl Acad Sci USA 102: 15545-15550, 2005.
31. Hemmati HD, Nakano I, Lazareff JA, Masterman-Smith M, Geschwind DH, Bronner-Fraser M and Kornblum HI: Cancerous stem cells can arise from pediatric brain tumors. Proc Natl Acad Sci USA 100: 15178-15183, 2003.
32. Smith AB, Rushing EJ and Smirniotopoulos JG: From the archives of the AFIP: lesions of the pineal region: radiologic-pathologic correlation. Radiographics 30: 2001-2020, 2010.
33. Fang AS and Meyers SP: Magnetic resonance imaging of pineal region tumours. Insights Imaging 4: 369-382, 2013.
34. Tong T, Zhenwei Y and Xiaoyuan F: MRI and 1H-MRS on diagnosis of pineal region tumors. Clin Imaging 36: 702-709, 2012.
35. Papaioannou G, Sebire NJ and McHugh K: Imaging of the unusual pediatric 'blastomas'. Cancer Imaging 9: 1-11, 2009.
36. Daumas-Duport C, Meder JF, Monsaingeon V, Missir O, Aubin ML and Szikla G: Cerebral gliomas: Malignancy, limits and spatial configuration. Comparative data from serial stereotaxic biopsies and computed tomography (a preliminary study based on 50 cases). J Neuroradiol 10: 51-80, 1983.
37. Price SJ, Jena R, Burnet NG, Hutchinson PJ, Dean AF, Peña A, Pickard JD, Carpenter TA and Gillard JH: Improved delineation of glioma margins and regions of infiltration with the use of diffusion tensor imaging: An image-guided biopsy study. AJNR Am J Neuroradiol 27: 1969-1974, 2006.
38. Korogi Y, Takahashi M and Ushio Y: MRI of pineal region tumors. J Neurooncol 54: 251-261, 2001.
39. Palled S, Kalavagunta S, Beerappa Gowda J, Umesh K, Aal M, Abdul Razack TP, Gowda V and Viswanath L: Tackling a recurrent pinealoblastoma. Case Rep Oncol Med 135435: 2014, 2014.
40. Gasparetto EL, Cruz LC Jr, Doring TM, Araújo B, Dantas MA, Chimelli L and Domingues RC: Diffusion-weighted MR images and pineoblastoma: Diagnosis and follow-up. Arq Neuropsiquiatr 66: 64-68, 2008.
41. Tate M, Sughrue ME, Rutkowski MJ, Kane AJ, Aranda D, McClinton LS, McClinton LS, Barani IJ and Parsa AT: The long-term postsurgical prognosis of patients with pineoblastoma. Cancer 118: 173-179, 2012.
42. Wang H, Zhang G, Zhang H, Zhang F, Zhou B, Ning F, Wang HS, Cai SH and Du J: Acquisition of epithelial-mesenchymal transition phenotype and cancer stem cell-like properties in cisplatin-resistant lung cancer cells through AKT/beta-catenin/Snail signaling pathway. Eur J Pharmacol 723: 156-166, 2014.
43. Heuberger J and Birchmeier W: Interplay of cadherin-mediated cell adhesion and canonical Wnt signaling. Cold Spring Harb Perspect Biol 2: a002915, 2010.
44. Kaufhold S and Bonavida B: Central role of Snail1 in the regulation of EMT and resistance in cancer: A target for therapeutic intervention. J Exp Clin Cancer Res 33: 62, 2014.
45. Huszthy PC, Daphu I, Niclou SP, Stieber D, Nigro JM, Sakariassen PO, Miletic H, Thorsen F and Bjerkvig R: In vivo models of primary brain tumors: Pitfalls and perspectives. Neuro Oncol 14: 979-993, 2012.
46. Tentler JJ, Tan AC, Weekes CD, Jimeno A, Leong S, Pitts TM, Arcaroli JJ, Messersmith WA and Eckhardt SG: Patient-derived tumour xenografts as models for oncology drug development. Nat Rev Clin Oncol 9: 338-350, 2012.
47. Bjerkvig R, Tonnesen A, Laerum OD and Backlund EO: Multicellular tumor spheroids from human gliomas maintained in organ culture. J Neurosurg 72: 463-475, 1990.
48. Wang J, Miletic H, Sakariassen PO, Huszthy PC, Jacobsen H, Brekkå N, Li X, Zhao P, Mørk S, Chekenya M, *et al*: A reproducible brain tumour model established from human glioblastoma biopsies. BMC Cancer 9: 465, 2009.